Nontrivial fusion of Majorana zero modes in interacting quantum-dot arrays

Bradraj Pandey [1,2] Satoshi Okamoto,[2] and Elbio Dagotto[1,2]

[1]*Department of Physics and Astronomy, The University of Tennessee, Knoxville, Tennessee 37996, USA*

[2]*Materials Science and Technology Division, Oak Ridge National Laboratory, Oak Ridge, Tennessee 37831, USA*

Motivated by recent experimental reports of Majorana zero modes (MZMs) in quantum-dot systems at the "sweet spot," where the electronic hopping t_h is equal to the superconducting coupling Δ, we study the time-dependent spectroscopy corresponding to the *nontrivial* fusion of MZMs. The term "nontrivial" refers to the fusion of Majoranas from different original pairs of MZMs, each with well-defined parities. We employ an experimentally accessible time-dependent real-space local density-of-states (LDOS) method to investigate the nontrivial MZM fusion outcomes in canonical chains and in a Y-shaped array of interacting electrons. In the case of quantum-dot chains where two pairs of MZMs are initially disconnected, after fusion we find equal-height peaks in the electron and hole components of the LDOS, signaling nontrivial fusion into both the vacuum I and fermion Ψ channels with equal weight. For π-junction quantum-dot chains, where the superconducting phase has opposite signs on the left and right portions of the chain, after the nontrivial fusion we observed the formation of an exotic two-site MZM near the center of the chain, coexisting with another single-site MZM. Furthermore, we also studied the fusion of three MZMs in the Y-shaped geometry. In this case, after the fusion we observed the novel formation of another exotic multisite MZM, with properties depending on the connection and geometry of the central region of the Y-shaped quantum-dot array.

I. INTRODUCTION

Majorana zero modes (MZMs) are attracting much attention due to their potential application in developing fault-tolerant quantum computation [1–3]. The MZMs follow non-Abelian statistics and allow the nonlocal encoding of quantum information, which makes them good candidates to utilize as qubits in topological quantum computations [3–5]. Recently, in coupled quantum-dot systems, a pair of localized MZMs were observed in the tunneling conductance measurements at the sweet spot $t_h = \Delta$, where the electronic hopping t_h and superconducting coupling Δ are equal in magnitude [6]. These quantum-dot systems [7–11] allow us to realize the idealized Kitaev chain with gate-tunable experimental parameters [12–14]. Realizing MZMs via quantum dots significantly reduces the problem of formation and detection of the MZMs, as compared to the more standard proximitized semiconducting nanowire systems, which are affected by random disorder [7,15].

This recent experimental progress in quantum-dot systems provides a platform to test the non-Abelian statistics of Majorana fermionic candidates [6,16]. Fusion and braiding are two fundamental characteristics of non-Abelian anyons [17,18]. The realization of MZMs at the sweet spot allows the study of the fusion and braiding of MZMs even in small

systems [6] (because in this case the MZMs are fully localized at a single site), as compared to the semiconducting nanowires that need a more extensive system. The sweet spot also facilitates analytical calculations for special cases [19,20]. The fusion of MZMs and the detection of their outcomes in quantum-dot experiments are expected to be easier than performing braiding of MZMs in other platforms.

The multiple fusion outcomes of MZMs, $\gamma \times \gamma = I + \Psi$, are related to their non-Abelian statistics [3], because two MZMs (γ) after fusion can result in either vacuum (I) or a fermion (Ψ) [17]. However, the fusion of MZMs can be designed in two ways, namely a "trivial" and a "nontrivial" procedure. In the trivial case, the fusion outcome is deterministic (either 100% I or 100% Ψ), as the fusion of MZMs occurs within the same pair with well-defined parity $+1$ or -1. This trivial fusion can be performed using just one pair of MZMs in a chain by moving one edge MZM towards the other edge MZM [21]. On the other hand, the nontrivial fusion refers to the fusion of Majoranas belonging to different initially disconnected pairs of MZMs each with predefined parities. In this nontrivial case, the fusion outcomes can yield both vacuum I and regular fermion Ψ with equal probability 50% [17,22]. To perform nontrivial MZMs, we need at least two pairs of MZMs, i.e., at least four MZMs. This paper mainly focuses on the time-dependent nontrivial fusion using two and three pairs of MZMs in models simulating interacting quantum-dot systems.

For the more canonical semiconductor nanowire setups, the detection of the fusion outcome of MZMs has been proposed by charge sensing based on dynamical Bogoliubov–de Gennes simulations [17,22,23]. Recently, in the context of coupled

quantum dots, the detection of the fusion of MZMs has been suggested using the parity readout of the systems [24]. Even without fusing the MZMs, by preparing the two pairs of MZMs in two different ways, the testing of fusion outcome has been proposed by observing the fermionic parity readout (deterministic or probabilistic) [24]. However, some studies indicate that "probabilistic parity measurements" can also occur for trivial low-energy modes [25,26]. Consequently, in the presence of low-energy modes, probabilistic parity measurements may yield false-positive signals in fusion experiments. Without careful manipulation of system parameters, these fusion experiments are not conclusive proof of the non-Abelian statistics of MZMs [25]. Compared to previous theoretical studies, we propose here detecting fusion outcomes using the time-dependent real-space electron and hole components of the local density-of-states methods [21] in both canonical chains and in Y-shaped arrays of interacting quantum dots. The quantum-dot system provides a very well-controlled setup, where the local control of individual quantum dots significantly reduces the damaging effect of disorder in detecting the MZMs [16]. The total local density-of-states [$LDOS(\omega, t)$] should be experimentally accessible via tunneling conductance measurements in the existing quantum-dot setups [6,27].

Motivated by the recent experimental realization of a minimal Kitaev chain in quantum dots coupled by a short superconductor-semiconductor hybrid (SC-SM) [6,28], here we study the nontrivial fusion of MZMs in quantum-dot arrays at the sweet spot ($t_h = \Delta$). In the quantum dot experiments, the hopping and superconducting coupling between the quantum dots are tunable by changing the electrostatic gate [12,14,29,30]. In this work, to observe the time-dependent nontrivial fusion, we tune the time-dependent hopping and superconducting coupling between quantum-dot arrays, where two different pairs of MZMs exist with predefined parities. We implement the time-dependent exact-diagonalization method using all the many-body states of interacting electrons of finite-size systems to study the spectroscopy of the nontrivial fusion of MZMs [21]. In the case of two one-dimensional chains with two pairs of MZMs [see Fig. 1(a)], we find equal height peaks in the electron and hole components of the $LDOS(\omega, t)$, showing the formation of both electron Ψ and vacuum channels. Surprisingly, due to the nonequilibrium effects and parity conservation of the time-evolving many-body state, we find the equal magnitude of electron and hole peaks at both $\pm\omega$ energies in $LDOS(\omega, t)$. In contrast to previous studies, we discuss the effect of repulsive Coulomb interaction on nontrivial fusion. We also present the time-dependent nontrivial fusion using a pair of quasi-MZMs away from the sweet spot and for a pair of MZMs at the sweet spots. In this scenario, namely when the left portion is away from the sweet spot and the right portion is at the sweet spot, we observe unequal peak heights in the electron and hole components of $LDOS(\omega, t)$ at $\pm\omega$ as time increases.

For the π-junction, where the two pairs of MZMs are initialized with opposite signs of the pairing amplitude after the fusion, we find that one of the central MZMs remains unaffected, while the second single-site MZM is transformed to a two-site nonlocal MZM. In fact, we find that this two-site MZM is formed after *tunneling* through the centrally localized
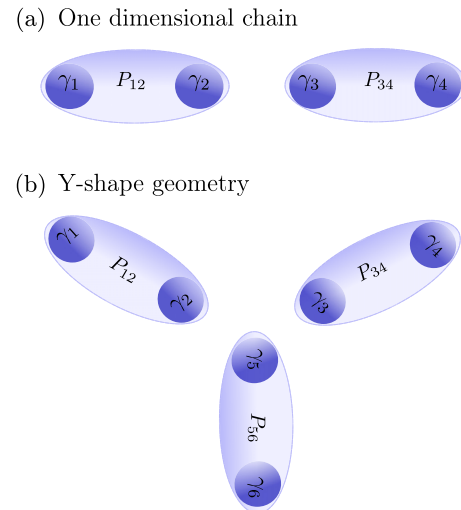

FIG. 1. Nontrivial fusion of Majoranas. (a) Schematic representation of two pairs of Majorana zero modes ([γ_1, γ_2] and [γ_3, γ_4]) in a quantum dot array. At time $t = 0$, the parities of the left $P_{12} = -i\langle\gamma_1\gamma_2\rangle$ and right $P_{34} = -i\langle\gamma_3\gamma_4\rangle$ pairs of MZMs are well defined. There is no hopping and no pairing coupling between the Majoranas γ_2 and γ_3. (b) Schematic representation of the three pairs of Majoranas zero modes in Y-shaped geometry. At time $t = 0$, the parities of three pairs of MZMs $P_{12} = -i\langle\gamma_1\gamma_2\rangle$, $P_{34} = -i\langle\gamma_3\gamma_4\rangle$, and $P_{56} = -i\langle\gamma_5\gamma_6\rangle$ are well defined. Initially, there is no hopping and pairing coupling between the three central Majoranas γ_2, γ_3, and γ_5. For nontrivial fusion, the time-dependent hopping and pairing amplitudes between the different pairs of MZMs were varied with time.

one-site MZM. The tunneling of *half* of the second MZM through another centrally localized one-site MZM is a novel effect in a strictly one-dimensional geometry [31].

Furthermore, we study the time-dependent fusion of an odd number (three) of Majoranas, where the three pairs of MZMs are initialized in a Y-shaped geometry [see Fig. 1(b)]. Surprisingly, during the fusion process we find zero energy peaks in the $LDOS(\omega, t)$ for three different central sites in addition to the electron and hole peaks at finite energies. After the fusion of Majoranas, we find the formation of an exotic multisite MZM. Interestingly, the nature of multisite MZMs depends on the connection and direction of the couplings near the center, which joins the legs of a Y-shaped quantum-dot array.

Last but not least, our results provide supportive evidence of the non-Abelian statistics of Majorana zero modes by probing the $LDOS(\omega, t)$ of nontrivial fusion. The most conclusive and definitive method to verify their non-Abelian statistics would be through "braiding" procedures [25]. Here, we are simply adapting to the novel experimental setups using quantum dots where peaks in the *conductance* are associated with Majoranas. These conductance peaks would appear in our setup as peaks at zero frequency in the local density of states. Future work will fully clarify the braiding procedure in the quantum dot setups, both experimentally and theoretically.

The organization of the manuscript is as follows. Section II contains the nontrivial fusion of Majorana zero modes for two one-dimensional chains with two pairs of MZMs. We divide

this section in two subsections where the two pairs of MZMs are initialized with the same signs for the pairing amplitudes (II A), and the opposite signs for the pairing amplitudes (II B). Section III describes the nontrivial fusion of three MZMs in a Y-shaped geometry. Finally, in Sec. IV we conclude our results.

II. NONTRIVIAL FUSION OF MZMs IN A ONE-DIMENSIONAL CHAIN

In this section, we will consider two one-dimensional quantum-dot arrays at the sweet spot, with the same sign for the superconducting phase ($\phi_1 = \phi_2 = 0$). These two left and right short wires are coupled through time-dependent hopping $[t_h(t)]$ and pairing $[\Delta(t)]$ terms, which can be tuned by changing the gate potential adiabatically. In the quantum-dot experiments, the hopping and pairing terms (and also their relative signs) between the two quantum dots are tuned by modifying the properties of Andreev bound states in a superconductor-semiconductor hybrid (SC-SM) [14,29,30]. These properties are controlled by an electrostatic gate connected to the SC-SM hybrid segment. The effective Hamiltonian for the quantum-dots arrays under the approximation of using only one level per quantum dot then becomes

$$H^L = \sum_{j=1}^{l-1} \left(-t_h c_j^\dagger c_{j+1} + e^{i\phi_1} \Delta c_j c_{j+1} + \text{H.c.} \right), \quad (1)$$

$$H^R = \sum_{j=l+1}^{2l} \left(-t_h c_j^\dagger c_{j+1} + e^{i\phi_2} \Delta c_j c_{j+1} + \text{H.c.} \right), \quad (2)$$

$$H^C(t) = \left(-t_h(t) c_l^\dagger c_{l+1} + \Delta(t) c_l c_{l+1} + \text{H.c.} \right). \quad (3)$$

The Coulomb interaction between quantum dots is the standard

$$H^{\text{Int}} = \sum_{j=1}^{2l} \left(V n_j n_{j+1} \right). \quad (4)$$

To perform future nontrivial fusion experiments, it is essential to prepare a high-quality initial state of two pairs of MZMs. This quality of MZMs can be compromised by the presence of disorder, interactions, or overlap between the MZMs within each pair involved in the fusion. In Fig. 2, we show the effect of repulsive Coulomb interactions V on the initial state with two pairs of MZMs for two different system sizes $L = 4$ and 12. We calculate the electron $[LD^e(\omega)]$ and hole parts $[LD^e(\omega)]$ of the local density of states separately for the central sites. Using the eigenvectors $|\Psi_m\rangle$ of the Hamiltonian H [Eqs. (1)–(4)], the electronic component of the local density of states $[LD_j^e(\omega)]$ for site j can be written as [21,32]

$$LD_j^e(\omega,) = -\frac{1}{\pi} \text{Im} \left(\sum_m \frac{|\langle \Psi_m | c_j | \Psi_1 \rangle|^2}{\omega + E_m - E_1 + i\eta} \right). \quad (5)$$

For the smaller system $L = 4$ (also known as the Poor Man's MZM pair), even a very small V leads to a shift in the zero-energy peaks of $LD_j^e(\omega)$ and $LD_j^e(\omega)$ from $\omega = 0$ to a finite value [Figs. 7(b) and 7(c)]. This is expected as the Poor Man's MZM lacks topological protection because of the overlap of wave functions [16,26]. Due to the smaller
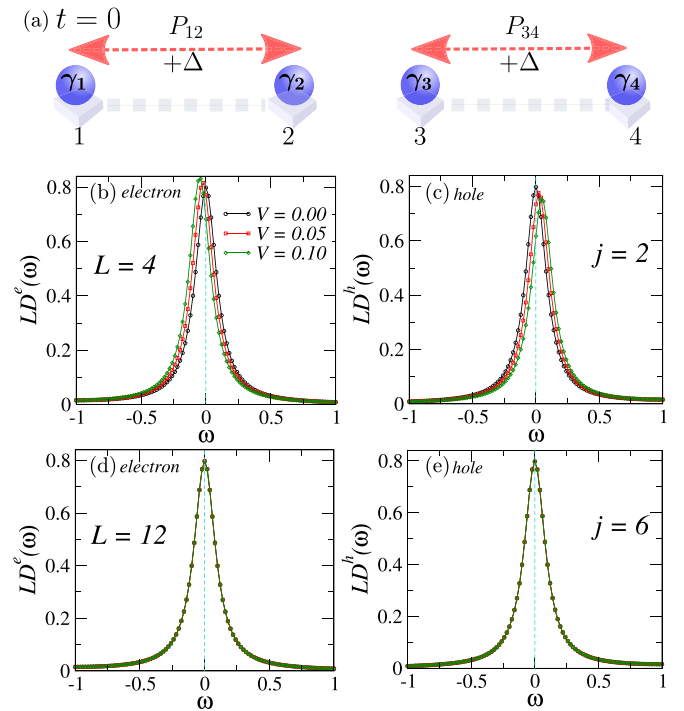

FIG. 2. (a) Schematic representation of two pairs of MZMs using a four-site quantum-dot array with the same left and right superconducting phases $\phi_1 = \phi_2 = 0$. (b,c) The electron $LD_j^e(\omega)$ and hole part $LD_j^e(\omega)$ of the local density of states at site $j = 2$ using $L = 4$ sites and different values of V. (d,e) The electron $LD_j^e(\omega)$ and hole part $LD_j^e(\omega)$ of the local density of states at site $j = 6$ using $L = 12$ sites and different values of V.

system size, the MZMs can hybridize if they involve more than one site, which lifts the ground-state degeneracy. Interestingly, for the system size $L = 12$ we find that the zero-energy peaks of $LD_j^e(\omega)$ and $LD_j^h(\omega)$ remains at $\omega = 0$ (with equal peak heights) for the smaller values of V [see Figs. 2(d) and 2(e)] as the wave-function overlaps are negligible. Using the full-diagonalization method, we find that the spectral weight at $\omega = 0$ in the $LD_j^e(\omega)$ and $LD_j^h(\omega)$ only arises from the fourfold-degenerate ground-state manifold, not from the higher-energy states above the gap. These results show that long enough system sizes (but still accessible by our techniques) give topological protection against the Coulomb repulsion due to exponentially decaying wave functions, and the quality of MZMs remains preserved at least for small values of V [33,34]. In the quantum-dot experiments, the Coulomb interaction V can be minimized by the superconducting segment in between the quantum dots [26].

A. The case $\phi_1 = \phi_2 = 0$

At time $t = 0$, there is no hopping and superconducting coupling between the two wires. As shown in Fig. 3(a), the system has two separate pairs of MZMs (γ_1, γ_2) and (γ_3, γ_4), with well-defined parities $P_{12} = -i\langle \gamma_1 \gamma_2 \rangle = -1$ and $P_{34} = -i\langle \gamma_3 \gamma_4 \rangle = -1$. The total parity (full system) of the initial many-body state can be calculated as $P_{\text{tot}} = e^{i\pi \sum_j n_j}$ [35]. The presence of four MZMs at $t = 0$ results in a fourfold-degenerate ground state, as we can potentially create two
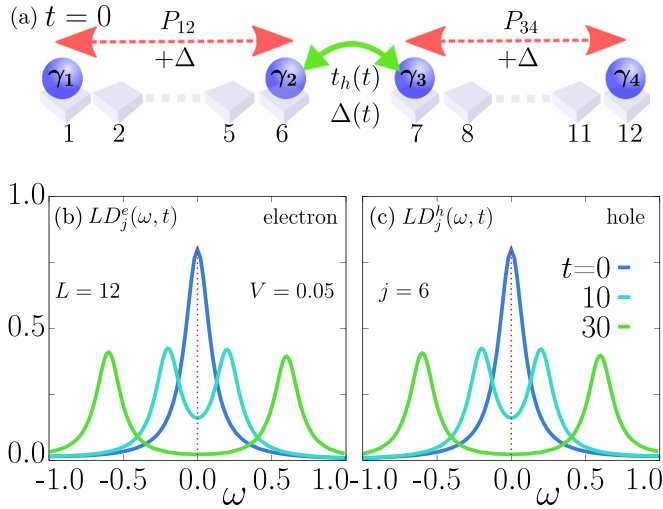
FIG. 3. (a) Schematic representation of two pairs of MZMs using a 12-site quantum dot array with the same left and right superconducting phases $\phi_1 = \phi_2 = 0$. At time $t = 0$, there is no hopping and no pairing coupling between the Majoranas γ_2 and γ_3. The time-dependent hopping and pairing coupling between sites $j = 6$ and 7 can be established by reducing the "barrier" between the left and right portions of the 12-site chain, leading to the nontrivial fusion of the central MZMs γ_2 and γ_3. (b) The electron component $LD^e(\omega, t, j)$ and (c) the hole component $LD^h(\omega, t, j)$ at site $j = 6$ and for different times t, at $V = 0.05$.

spinless fermions by combining these four MZMs in pairs (thus we have degeneracy $2^2 = 4$). Fusing the MZMs within the same pair (with parity -1 as an example), namely γ_1 and γ_2 or γ_3 and γ_4, using a height-variable potential wall in between them, results in the formation of a full electron (trivial fusion) [21]. This trivial fusion reveals only one fusion channel Ψ with deterministic formation of a full electron. On the other hand, the nontrivial fusion of our focus in this paper is expected to produce both fusion channels and a more exotic intermediate dynamics.

In the real experiments of a fusion of MZMs, one needs to change the hopping and pairing amplitude as a function of time close to the adiabatic limit in a dynamical way. Namely, in the real experiments the outcome depends on the initial condition and on the speed of the process. Here, we perform time-dependent fusion of MZMs by changing the hopping according to the formula $t_h(t) = t_h(T)\frac{n\delta t}{\tau}$, where $1/\tau$ is the quenched rate, $\delta t = 0.001$ is the small time step we used, and n is the integer number of those steps, such that the $t_h(t)$ at sites $j = 6$ and 7 increases approximately linearly from 0 to 1 in a time $\tau = 100$. At final time $t = T$, the time-dependent hopping becomes equal to $t_h(T) = 1$. For the time evolution, we chose the initial many-body state $|\Psi(0)\rangle$ with total parity $P_{\text{tot}} = +1$ (this parity is chosen because it corresponds to the ground state at nonzero V). To observe the fusion outcomes at intermediate time t, first, we time-evolve the initial wave function $|\Psi(0)\rangle$ up to time t using the time-dependent Hamiltonian $H(t)$ as $|\Psi(t)\rangle = \mathcal{T} \exp\left(-i\int_0^t H(s)ds\right)|\Psi(0)\rangle$, where $\mathcal{T}$ is the time ordering operator [36]. Next, we calculate the double-time Green function $G(t, t')$ [37] using the instan-

taneous Hamiltonian $H_f = H(t = t_f)$ at time $t = t_f$:

$$G_j^{\text{elec}}(t, t') = \langle\Psi(t)|c_j^\dagger e^{iH_f t'} c_j e^{-iH_f t'}|\Psi(t)\rangle. \quad (6)$$

The time-dependent $LD_j^e(\omega, t)$ for the electronic part of the local density of states is the Fourier transform of the local Green function at site j with respect to t'. Using the eigenvectors $|\phi_m\rangle$ of the instantaneous Hamiltonian $H(t)$ and $|\Psi(t)\rangle$ at time t, the electronic component of $LD_j(\omega, t)$ at site j can be written as $LD_j^e(\omega, t)$ [21]

$$= \frac{-1}{\pi}\text{Im}\left(\sum_{m,n} \frac{\langle\Psi(t)|c_j^+|\phi_n\rangle\langle\phi_n|c_j|\phi_m\rangle\langle\phi_m|\Psi(t)\rangle}{e_n - e_m + \omega + i\eta}\right). \quad (7)$$

The broadening parameter was fixed to $\eta = 0.1$ throughout. e_n and e_m denote eigenvalues of the instantaneous Hamiltonian $H(t)$. Similarly, the hole component of $LD_j(\omega, t)$ at site j can be written as $LD_j^h(\omega, t)$ [21]:

$$= \frac{-1}{\pi}\text{Im}\left(\sum_{m,n} \frac{\langle\Psi(t)|\phi_n\rangle\langle\phi_n|c_j|\phi_m\rangle\langle\phi_m|c_j^\dagger|\Psi(t)\rangle}{e_n - e_m + \omega + i\eta}\right). \quad (8)$$

Interestingly, with an increase in the couplings $t_h(t)$ and $\Delta(t)$, the electron $LD_j^e(\omega, t)$ and hole $LD_j^h(\omega, t)$ both show equal-height subgap peaks close to $\omega = \pm t_h(T)\frac{2t}{\tau}$ [in the rest of the paper, we use $t_h(T) = 1$] for $V = 0.05$, reflecting the formation of equal amounts of electron and hole at positive and negative values of ω [see Figs. 3(b) and 3(c)]. The appearance of equal magnitude electron and hole components at both frequencies $\omega = \pm 2t/\tau$ is clearly a nonequilibrium effect and it is influenced by the conservation of total parity of $|\Psi(t)\rangle$. Due to this dynamics, the time-evolving wave function $|\Psi(t)\rangle$ has an equal overlap with low-energy states $|\Psi_1\rangle$ and $|\Psi_4\rangle$ with the same total parity $P = +1$ (see Appendix C). This allows for similar spectral weights close to $\omega = -2t/\tau$ in $LD_j^e(\omega, t)$ (transition from state $m = 1$ to $n = 4$) and $LD_j^h(\omega, t)$ (from state $m = 2$ to $n = 3$), and also similar spectral weights close to $\omega = +2t/\tau$ in $LD_j^e(\omega, t)$ (resulting from a transition from state $m = 3$ to $n = 2$) and in $LD_j^h(\omega, t)$ (from state $m = 4$ to $n = 1$).

The equal superposition of two low-energy many-body states in $|\Psi(t)\rangle$ even for large $\tau = 100$ [we have also checked for the case $\tau = 500$ and the results are the same (see Appendix D)] is a unique property of nontrivial fusion. In the trivial fusion for the larger τ, the time-evolving wave function $|\Psi(t)\rangle$ overlaps with only one low-energy state of the instantaneous ground-state manifold of the time-evolving Hamiltonian. Introducing a time-dependent hopping $t_h(t)$ and pairing $\Delta(t)$, the fuse of the MZMs γ_2 and γ_3 occurs nontrivially because the MZMs are from different pairs. The $t_h(t)$ and $\Delta(t)$ allows for tunneling of a single electron (or a pair of electrons) from the left to the right chain portions during the fusion process, which changes the individual parities of those left and right quantum-dot segments, but the total parity of the many-body state $|\Psi(t)\rangle$ remains the same [38]. This results in the formation of both fermion Ψ and vacuum I channels, after fusion of γ_2 and γ_3 nontrivially (see Appendix A for more details). At the final time $t = T$, the system has two MZMs (γ_1 and γ_4) at the left and right edge of the chain [see Fig. 3(b)].
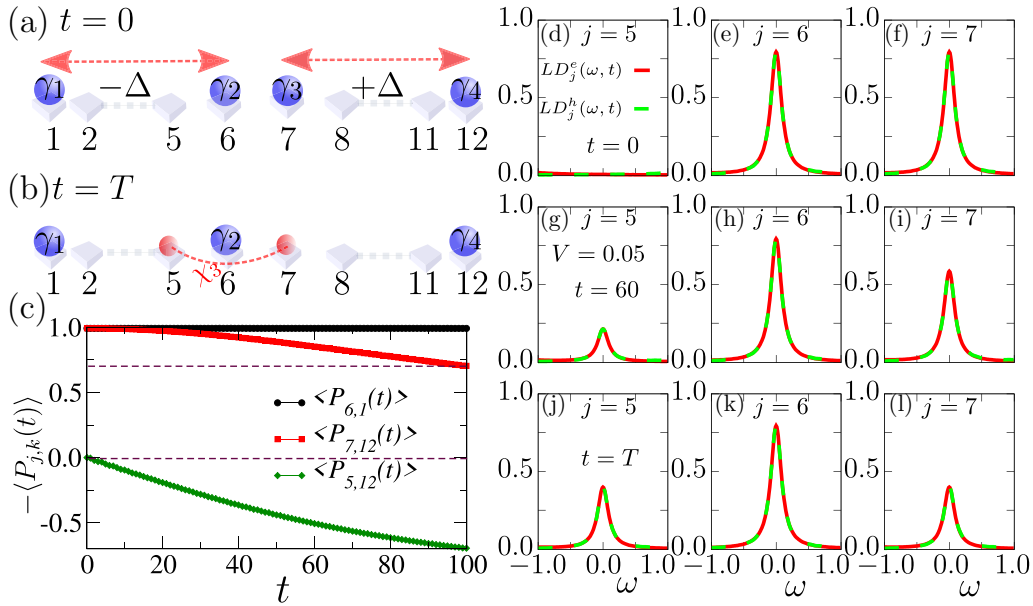
FIG. 4. (a) Schematic representation of two pairs of MZMs [(γ_1, γ_2) and (γ_3, γ_4)]: at time $t = 0$, the left part has pairing coupling strength $-\Delta$, while the right part has pairing coupling strength $+\Delta$. (b) Pictorial representation for the formation of a multisite MZM (χ_3) at time $t = T$. (c) Time-dependent parity $-\langle P_{j,k}(t)\rangle$ as a function of time t for different pairs of Majoranas and at $V = 0.05$. The electron and hole components of the time-dependent local density of states $LD_j^e(t)$ and $LD_j^h(t)$ at time $t = 0$ and for sites (d) $j = 5$, (e) $j = 6$, and (f) $j = 7$. The $LD_j^e(t)$ and $LD_j^h(t)$ at intermediate time $t = 60$ and for sites (g) $j = 5$, (h) $j = 6$, and (i) $j = 7$. The $LD_j^e(t)$ and $LD_j^h(t)$ at the final time $t = T$ and for sites (j) $j = 5$, (k) $j = 6$, and (l) $j = 7$.

In summary, we have found an equal spectral weight for electron and hole components in the time-dependent local density of states during the nontrivial fusion process of Majoranas from different pairs. Interestingly, the time-evolving state becomes an almost equal-linear superposition of two low-energy states, even for larger values of τ. The appearance of equal height peaks of electron and hole in the local density of states signals the nontrivial nature of Majorana fermions. In the case of fusion involving two pairs of MZMs, where the two MZMs of the left pair are already slightly hybridized (for $\Delta_1 = 0.7$ and $\Delta_2 = 1.0$), this leads to an asymmetry in the peak heights close to $\omega = \pm 2t/\tau$ (see Appendix A). In other words, there is a formation of unequal-height electron and hole peaks around $\omega = \pm 2t/\tau$, which is clearly different from the case of an initial state with nonoverlapping pairs of MZMs.

B. The case $\phi_1 = \pi$ and $\phi_2 = 0$

In this subsection, we will study the Majorana fusion in a π-junction setup. To form a π-junction between the right and left quantum-dot arrays, we consider two pairs of MZMs, in this case with opposite signs of the pairing terms ($-\Delta$ for the left array and $+\Delta$ for the right array). The MZM in the left quantum-dot array has definite parity $P_{6,1} = -i\langle\gamma_6\gamma_1\rangle = -1$, and that in the right pair has definite parity $P_{7,12} = -i\langle\gamma_7\gamma_{12}\rangle = -1$ as well [see Fig. 4(a)]. At $t = 0$ there are no hopping and pairing terms between the left and right arrays (the system has a mirror symmetry with respect to a line passing in between sites $j = 6$ and 7).

Next, we turn on the time-dependent hopping (t_h) and pairing $\Delta(t)$ terms (with zero phase factor as an example)

between the left and right arrays, which effectively makes a time-dependent π-junction quantum-dot array. Note that the introduction of time-dependent $\Delta(t)$ terms with zero phase factor breaks the initial global mirror symmetry about the line in between the sites $j = 6$ and 7. The choice of positive $\Delta(t)$ leads to the formation of a π-junction at site $j = 6$ (i.e., for $j \leqslant 6$ the pairing term is $\Delta < 0$ and for $j > 6$ it has positive $\Delta > 0$). To observe the behavior of the central Majoranas γ_2 and γ_3, we calculate the time-dependent electron $LD_j^e(t)$ and hole $LD_j^h(t)$ portions of the local density of states for sites $j = 5$, 6, and 7. At $t = 0$ the electron $LD_j^e(t)$ and hole $LD_j^h(t)$ portions of the local density of states show equal height peaks at $\omega = 0$ for the sites $j = 6$ and 7, which indicate the presence of two localized MZMs [see Figs. 4(d)–4(f)].

Increasing time to $t = 60$ [Figs. 4(g)–4(i)], the peak heights of $LD_j^e(t)$ and $LD_j^h(t)$ increase for site $j = 5$, remain *constant* for site $j = 6$, and decrease for site $j = 7$. This spectral weight shift suggests the *tunneling* of MZM γ_3 from site $j = 7$ to 5. Note that the heights of the peaks at $\omega = 0$, for the electron $LD_j^e(t)$ and hole $LD_j^h(t)$ parts of the local density of states, are almost equal for each site for all times t. We also find that the spectral weight at $\omega = 0$ mainly arises from the low-energy subspace of fourfold degenerate states. The equal contribution of electron and hole parts of the local density of states at $\omega = 0$ for these central sites shows the presence of Majorana zero modes at sites $j = 5$, 6, and 7.

At the final time $t = T = 100$, the $LD_j^e(t)$ and $LD_j^h(t)$ have almost equal height peaks for sites $j = 5$ and 7, and the total spectral weights on these two sites is close to localized on-site MZM, confirming the formation of the multisite MZM χ_3 [see Fig. 4(b)]. The $LD_j^e(t)$ and $LD_j^h(t)$ for site $j = 6$ all

remain constant up to time $t = T$. Thus, the transfer of spectral weight from site $j = 7$ to 5 at $\omega = 0$ hints at a tunneling effect of half of the MZM γ_3 from site $j = 7$ to site $j = 5$, leading to the formation of a multisite MZM χ_3.

Interestingly, the four low-energy states remains degenerate, even after switching the time-dependent hopping $t_h(t)$ and pairing $\Delta(t)$ terms between the left and right arrays, showing the presence of a total of four MZMs in the system. We also find that the time-evolving wave function $|\Psi(t)\rangle = u|\Psi_1\rangle + v|\Psi_4\rangle$ becomes a superposition of two low-energy degenerate ground states with the same total parity (see Appendix C). The amplitudes u and v depend on the tunneling of the MZM γ_3 from site $j = 7$ to site $j = 5$ (for $L = 10$ site and time $t = 20$, $|u|^2 = 0.8$ and $|v|^2 = 0.2$). These amplitudes u and v remain the same for different values of large τ. Furthermore, to confirm the tunneling of MZM γ_3, we also calculate the time-dependent parity $\langle P_{j,k}(t)\rangle = -i\langle \Psi(t)|\gamma_j\gamma_k|\Psi(t)\rangle$ for different pairs of Majoranas. As shown in Fig. 4(c), the observable $\langle P_{6,1}(t)\rangle$ remains constant with time, showing that the MZM γ_2 remains localized at site $j = 6$ without any change in parity of the pair (γ_1, γ_2). Meanwhile, $\langle P_{7,12}(t)\rangle$ starts decreasing and approaches the value $1/\sqrt{2}$ at time $t = T$. On the other hand, $\langle P_{5,12}(t)\rangle$ becomes nonzero as time increases and approaches $-1/\sqrt{2}$. Once again, these results suggest the formation of a multisite MZM with the form $\chi_3 = -\frac{1}{\sqrt{2}}\gamma_5 + \frac{1}{\sqrt{2}}\gamma_7$, where one component of χ_3 appears due to tunneling of γ_3 initially localized on site $j = 7$.

For the ground state of a one-dimensional Kitaev wire with a π-junction, there are a total of four MZMs. For the system considered in Fig. 4, at the final time $t = T$, the system forms a π-junction at site $j = 6$. To understand the behavior of the central MZMs, using just three central sites ($j = 5$, 6, and 7) near the junction, we can write the Hamiltonian for the central region as (with $\phi_1 = \pi$ and $\phi_2 = 0$ for the two central bonds, respectively)

$$H^{\mathrm{III}} = -2i\Delta\left(\gamma_5^B\gamma_6^B + \gamma_7^A\gamma_6^B\right), \qquad (9)$$

where we have used the relations $c_5 = \frac{1}{\sqrt{2}}e^{-i\phi_1/2}(\gamma_5^A + i\gamma_5^B)$, $c_6 = \frac{1}{\sqrt{2}}(\gamma_6^A + i\gamma_6^B)$, and $c_7 = \frac{1}{\sqrt{2}}e^{-i\phi_2/2}(\gamma_7^A + i\gamma_7^B)$. Interestingly, the Majorana operator γ_6^A is absent in the Hamiltonian, showing that γ_6^A is a single-site MZM mode at site 6. The form of the Hamiltonian also suggests that one localized mode, γ_6^A, does not interact with any other Majorana zero mode, which could be the reason for localization of the initial Majorana mode located at site $j = 6$. Our recent work, using symmetry arguments, shows that for the two wires (each carrying a pair of MZMs) with a phase difference of π, the central MZMs are protected by mirror symmetry. The central MZMs do not fuse as they belong to different quantum numbers [39]. After diagonalizing the Hamiltonian H^{III}, we find that a multisite MZM $\chi_3 = -\frac{1}{\sqrt{2}}\gamma_5 + \frac{1}{\sqrt{2}}\gamma_7$ resides at sites $j = 5$ and 7 (see the SM of Ref. [20] for a more detail calculation). These ground-state results indicate that out of an initial total of four single-site MZMs, there are now three single-site local MZMs (two localized at edge end sites and one at central site j) and one multisite MZM with the form $\chi_3 = -\frac{1}{\sqrt{2}}\gamma_j + \frac{1}{\sqrt{2}}\gamma_{j+2}$.

In summary, the Majoranas near the π-junction do not fuse. Instead, one MZM remains a localized single-site MZM, and

another transforms into a multisite MZM (located on two sites with equal amplitude). The tunneling of half of the second MZM through the centrally localized one-site MZM in a strict one-dimensional geometry is an interesting dynamical effect. This partial tunneling of a Majorana leads to the time-evolving wave function in a superposition of two low-energy degenerate states (with the same total parity).

III. NONTRIVIAL FUSION OF MZMs IN Y-SHAPED QUANTUM DOT ARRAYS

This section will study the fusion of three MZMs from different pairs, further increasing the complexity of the problem. The presence of multiple Majoranas can occur in topological materials or in quantum circuits experiments. The overlap between odd and even numbers of Majoranas can give different behavior in the tunneling spectra [40]. Here, we simulate the overlap between an odd number (three) of MZMs as a function of time, starting with fully separated MZMs. We consider a Y-shaped geometry consisting of three quantum-dot chains at the sweet spot and with the same superconducting phase $\phi_1 = \phi_2 = \phi_3 = 0$ at each arm. At time $t = 0$, there is no hopping and superconducting coupling between these three quantum-dot arrays. As shown in Fig. 5(a), the system has three pairs of Majorana zero modes (γ_1, γ_2), (γ_3, γ_4), and (γ_5, γ_6), with well-defined initial parities $P_{12} = -i\langle\gamma_1\gamma_2\rangle = +1$, $P_{34} = -i\langle\gamma_3\gamma_4\rangle = +1$, and $P_{56} = -i\langle\gamma_5\gamma_6\rangle = +1$. The six Majorana modes at the sweet spot ($t_h = \Delta = 1$ and $V = 0$) give rise to an eightfold-degenerate ground state, because we can form three nonlocal spinless fermions (which give rise to $2^3 = 8$-fold degeneracy). Within an eightfold-degenerate ground state, four states have individual total parity $P = +1$ and the remaining four have parity $P = -1$. Using the fourfold-degenerate ground state with the same fixed parity, one can encode two topological qubits, which can display all the basic operations for topological quantum computation [41].

The Hamiltonian for the Y-shaped quantum-dot array (with $\phi_1 = \phi_2 = \phi_3 = 0$ at each arm) can be divided into four different parts. The Hamiltonian for each arm can be written as

$$H^{\mathrm{I}} = \sum_{j=1}^{l-1} \left(-t_h c_j^\dagger c_{j+1} + \Delta c_j c_{j+1} + \mathrm{H.c.}\right), \qquad (10)$$

$$H^{\mathrm{II}} = \sum_{j=l+1}^{2l-1} \left(-t_h c_j^\dagger c_{j+1} + \Delta c_j c_{j+1} + \mathrm{H.c.}\right), \qquad (11)$$

$$H^{\mathrm{III}} = \sum_{j=2l+1}^{3l-1} \left(-t_h c_j^\dagger c_{j+1} + \Delta c_j c_{j+1} + \mathrm{H.c.}\right). \qquad (12)$$

Moreover, in order to fuse the MZMs from different pairs, first we switch on the time-dependent pairing $\Delta(t)$ and hopping $t_h(t)$ terms between each arm. In practice, we tune the time-dependent pairing and hopping terms as $\Delta(t) = t_h(t) = t_h(T)\frac{n\delta t}{\tau}$ between the central three MZMs $(\gamma_2, \gamma_3, \gamma_5)$. We used $\tau = 100$ and other parameters as described in the previous cases. T is the final time such that $\Delta(t) = t_h(t) = 1$ at $t = T = 100$. The time-dependent Hamiltonian coupling the
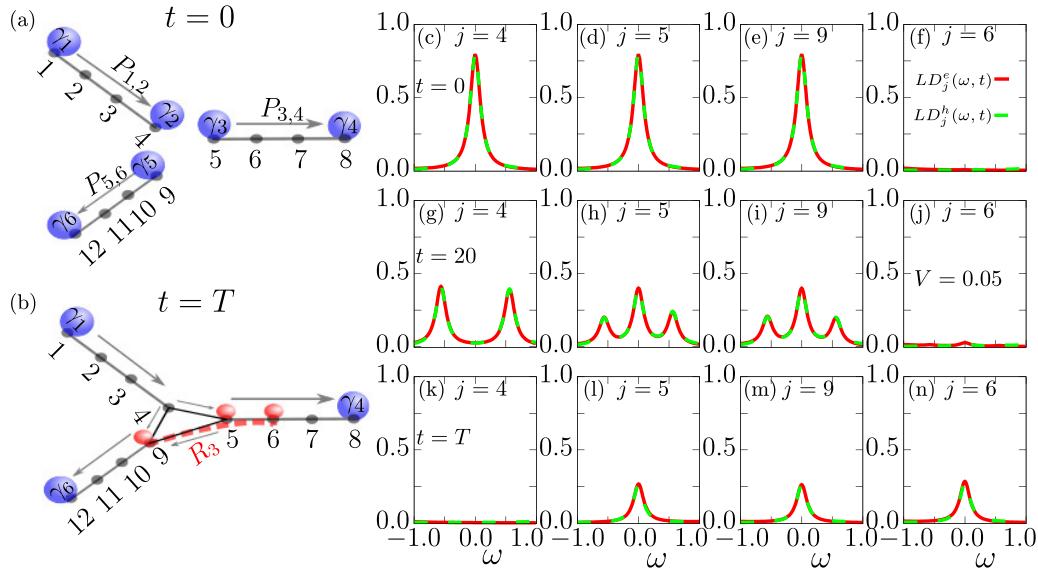
FIG. 5. (a) Schematic representation of three pairs of Majorana zero modes in a Y-shaped Kitaev wire. At $t = 0$, each pair has fixed fermionic parity $P_{1,2} = +1$, $P_{3,4} = +1$, and $P_{5,6} = +1$. The direction of the arrows denotes the directions of the pairing terms Δ and site index j in each wire. (b) Pictorial representation of the formation of the multisite MZM R_3 after the fusion of the three central MZMs at time $t = T$, after the adiabatic process ends. The time-dependent electron $LD_j^e(\omega, t)$ and hole $LD_j^h(\omega, t)$ portions of the local density of states at time $t = 0$ and for sites (c) $j = 4$, (d) $j = 5$, (e) $j = 9$, and (f) $j = 6$. The $LD_j^e(\omega, t)$ and $LD_j^h(\omega, t)$ for the intermediate time $t = 20$ and for sites (g) $j = 4$, (h) $j = 5$, (i) $j = 9$, and (j) $j = 6$. The $LD_j^e(\omega, t)$ and $LD_j^h(\omega, t)$ for the final time $t = T$ and for sites (k) $j = 4$, (l) $j = 5$, (m) $j = 9$, and (n) $j = 6$. These numerical calculations were performed using $L = 12$ sites and $t_h = \Delta = 1$, $V = 0.05$.

arm edges is written as

$$
\begin{aligned}
H^C(t) = &-t_h(t)c_l^\dagger c_{l+1} + \Delta(t)c_l c_{l+1} + \text{H.c.} \\
&-t_h(t)c_{l+1}^\dagger c_{2l+1} + \Delta(t)c_{l+1} c_{2l+1} + \text{H.c.} \\
&-t_h(t)c_l^\dagger c_{2l+1} + \Delta(t)c_l c_{2l+1} + \text{H.c.} \quad (13)
\end{aligned}
$$

Using the above Hamiltonian $H = H^{\text{I}} + H^{\text{II}} + H^{\text{III}} + H^C(t)$, we performed the time evolution starting from the ground state with total parity $P = +1$, and we calculated the electron $LD_j^e(\omega, t)$ and hole $LD_j^h(\omega, t)$ portions of the local density of states for various times t. At $t = 0$, we find that the central edge sites $j = 4$, 5, and 9 in $LD_j^e(\omega, t)$ and $LD_j^h(\omega, t)$ have sharp peaks at $\omega = 0$ [Figs. 5(c)–5(f)]. Introducing a time-dependent hopping and pairing term leads to the simultaneous fusion of three central MZMs (γ_2, γ_3, γ_5), the three belonging to different original MZM pairs. The fusion of central MZMs leads to a split in the initial eightfold-degenerate ground state into two sets of low-energy fourfold-degenerate states.

As shown in Fig. 5(g), the time-dependent electron $LD_j^e(\omega, t)$ and hole $LD_j^h(\omega, t)$ portions of the local density of states at time $t = 20$, for site $j = 4$, show peaks close to $\omega = \pm \frac{3t}{\tau}$, indicating the formation of both electron and hole for positive and negative frequencies. Using Eqs. (6) and (7), we find the spectral weights at $\omega = \pm \frac{3t}{\tau}$ in the electron and hole parts of $LD_j(\omega, t)$ arising from the transition between the splitted two-set of fourfold-degenerate states (mainly $n = 2$ to $m = 6$ or $n = 1$ to $m = 5$). In fact, the time-evolving state $|\Psi(t)\rangle$ becomes a superposition of four states (two from the lower fourfold-degenerate part and the remaining two from

the other fourfold states of the eightfold low-energy states) of the instantaneous Hamiltonian.

At sites $j = 5$ and 9 [Figs. 5(h) and 5(i)], the $LD_j^e(\omega, t)$ and $LD_j^h(\omega, t)$ show peaks at $\omega = 0$ and also close to $\omega = \pm \frac{3t}{\tau}$, with equal spectral weight of the electron and hole portions of the time-dependent local density of states. These results for the sites $j = 5$ and 9 show that the MZMs still survive for these sites, and in addition there is a formation of electron and hole close to $\omega = \pm \frac{3t}{\tau}$ due to the partial fusion of MZMs. Interestingly, for site $j = 6$, a small peak appears at $\omega = 0$ [Fig. 5(j)]. With a further increase in time, we find for sites $j = 5$ and 9 the peaks at $\omega = 0$ decrease with time. On the other hand, for site $j = 6$ the peak strength at $\omega = 0$ increases with increasing time t. These results show the *transfer* of spectral weight from the central sites ($j = 5$ and 9) to the site $j = 6$. For the final time after the adiabatic process, $t = T$, the $LD_j^e(\omega, t)$ and $LD_j^h(\omega, t)$ show almost equal-height peaks at $\omega = 0$ for the three central sites $j = 5$, 9, and 6; see Figs. 5(l)–5(n). These results indicate the formation of an equal amount of electron and hole, and, surprisingly, one multisite MZM after the fusion of three central MZMs. In other words, we unveiled an interesting result that the fusion of three one-site MZMs leads to a single MZM spread on three sites.

In summary, in comparison to the fusion of two MZMs (even numbers), the fusion of three MZMs (odd numbers) gives rise to a novel multisite MZM. The local density of states shows peaks at $\omega = 0$ for three different central sites. Note that the multisite MZM position depends on the pairing terms' direction. The appearance of a multisite MZM near the central part is mainly due to the different coupling directions (effectively a π-junction) at the trijunction [see Fig. 5(b)].

IV. SUMMARY AND OUTLOOK

In this paper, we studied the nontrivial fusion of Majorana zero modes in canonical chains, as well as in a Y-shaped array of interacting quantum dots close to the sweet spot in parameter space. We examined the real-time dynamics of the local density of states to reveal the nature of the nontrivial fusion of MZMs. The Majoranas were initialized in pairs with definite parity in separate quantum-dot arrays. Varying the time-dependent hopping and pairing terms between the different quantum-dot arrays, we carry out the fusion of Majoranas from different pairs (nontrivial fusion). We observed the fusion outcomes by calculating the time-dependent electron and hole part of the local density of states. Several interesting results were unveiled:

(i) In the case of a one-dimensional chain with the same phase on each left and right wire, we demonstrated the formation of both an electron and a hole close to $\omega = \pm 2t/\tau$ in equal magnitude for small values of Coulomb interactions. The formation of equal height peaks of the electron and hole at each $\omega = \pm 2t/\tau$ value is a dynamical effect and reveals the nontrivial nature of the MZMs fusion. In fact, we find that the time-evolving states becomes an equal superposition of two states (with the same parities). This nonequilibrium effect is unique in the case of the nontrivial fusion. For the trivial fusion, the time-evolving states overlap with only one state of the instantaneous Hamiltonian. We also explored the nontrivial fusion using a pair of overlapping quasi-MZMs away from the sweet spot and a pair of nonoverlapping MZMs at the sweet spot. In this case, we find an asymmetry in the peak height of the electron and hole portions of the local density of states at $\omega = \pm 2t/\tau$. The unequal-peak heights varying time in the electron and hole part of the local density arises from having an initial state with unequal contributions of the electron and hole components of the quasi-MZMs.

(ii) On the other hand, quite interesting results were found for the case of a π-junction (with opposite phase on each left and right wire) because the Majoranas do not fuse with one another. Instead they formed a multisite MZM residing on two sites near an independent localized one-site central MZM. The time-average parity and time-dependent local density of states reveals that the one-site MZM at the edge (near the center) of the left array does not fuse with other MZMs and remains localized on the same edge site. Surprisingly, half of the MZM of the right quantum-dot array (near the center) *tunnels* through the localized one-site MZM and forms a multisite MZM. The tunneling of half of the MZM even in a strict one-dimensional geometry is a quite novel effect. The tunneling of the MZM also makes the time-evolving state become a superposition of two states from the fourfold-degenerate ground-state manifold of the instantaneous Hamiltonian even for a smaller quench rate. The amplitude of the two states in the time-evolving state depends on the amount of tunnel MZM through the centrally localized MZM. In the quantum-dot system, the π-junction can be experimentally achieved by applying a magnetic flux through a superconducting loop that connects the two hybrid segments of such a system [42]. Additionally, the relative sign of hopping and superconducting coupling between the quantum dots can also be altered using an electrostatic gate attached to the hybrid region, even without any application of magnetic flux [30].

(iii) For the fusion of MZMs in a Y-shaped quantum-dot array, where the MZMs are coupled through time-dependent hopping and pairing terms in a triangular geometry, we show the formation of an exotic multisite MZM after the fusion of three central MZMs from different pairs. Interestingly, the time-evolving state becomes a superposition of four states of an instantaneous Hamiltonian (two from the lower four-fold degenerate states and the other two from the higher fourfold-degenerate states), due to the nontrivial fusion and the formation of multisite MZMs. In general terms, the nature and behavior of the central multisite MZMs are dependent on the geometry and direction of the pairing terms of quantum-dot arrays. The knowledge of the characteristics of the central multisite MZMs is important for the braiding of MZMs in dynamical and realistic settings, where the exchange of MZMs is performed by moving the MZMs adiabatically. In comparison to the previously studied MZM fusion in the noninteracting single-particle picture, here we do not find any density fluctuations during the nontrivial fusion of MZMs (in one-dimensional geometry), using the time-evolving many-body wave function. The formation of the electron and hole clearly appears in the electron and hole parts of the time-dependent local density of states. The local density of states can be measured in tunneling spectroscopy in quantum-dot experiments.

The study of nontrivial fusion is related to non-Abelian statistics and can be performed in quantum-dot setups. For successful fusion experiments, it is crucial to carefully consider the effects of interactions, disorder, and system size, because trivial low-energy modes could produce false-positive results [25,26]. Our results indicate that even small intersite Coulomb interactions can be destructive for the Poor Man's Majorana zero modes, causing all four MZMs to move away from zero energy for short chain systems. Fortunately, such an effect is absent for longer chains, showing that the topological protection increases with system size.

Our time-dependent results for the electron and hole components of the local density of states suggest that separately measuring the electron and hole portions of such a local density of states could aid in distinguishing the fusion outcomes from trivial low-energy modes with unequal superposition of electron and hole states [43]. However, the tunneling experiments generally measure the total local density of states, making it challenging to differentiate between fusion outcomes, low-energy modes, and topological MZMs. Fortunately, recent advancements in quantum-dot systems provide a well-controlled setup, and the effective local gate control of individual quantum dots significantly reduces the effect of disorder or low-energy modes, making it feasible to measure MZMs more accurately than in nanowire systems [16]. We believe that our novel theoretical results for the nontrivial fusion of Majoranas in the one-dimensional chain and in the Y-shaped geometries can be realized using the recently developed quantum-dot setups. Our prediction of the fusion outcome, based on the time-dependent local-density-of-states method, is accessible to present-day experimental capabilities [6]. Braiding experiments using Y-shaped [20] or X-shaped [39] quantum dots should provide more conclusive and definitive evidence of MZMs and their non-Abelian properties, but such efforts will be pursued in the future [26].
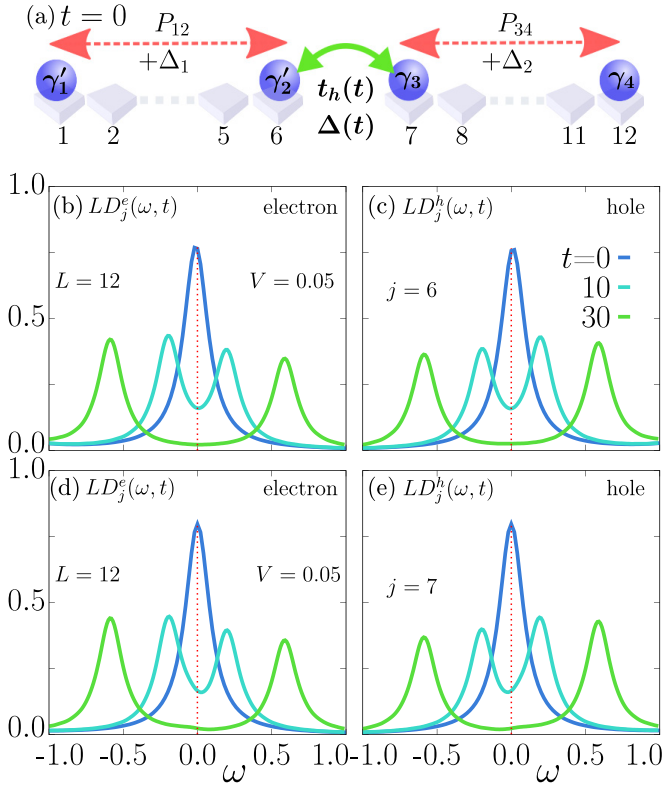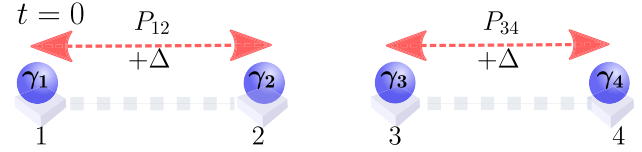
FIG. 7. Schematic representation of two pairs of MZMs using a four-site quantum-dot array with the same left and right superconducting phases $\phi_1 = \phi_2 = 0$.

hopping and pairing terms between the left and right quantum-dot segments in order to fuse the quasi-MZM γ_2' (at $j = 6$) and MZM γ_3 (at site $j = 7$) nontrivially, as described in the main text. Interestingly, in this case with increasing time, we find unequal-height electron and hole peaks close to $\omega = \pm 2t/\tau$. The unequal peak height comes from the fact that for this case the time-evolving wave function $|\Psi(t)\rangle$ has an unequal overlap with the low-energy states $|\Psi_1\rangle$ and $|\Psi_4\rangle$, which is quite different from the nontrivial fusion, where the left and right pairs of MZMs were initialized at the sweet spot $\Delta_1 = \Delta_2 = 1$. This shows that our time-dependent results for the electron and hole components of the local density could be used to distinguish the fusion outcomes from trivial low-energy modes (which appears after hybridization of two MZMs in the same region). However, we find that the total local density of states at $\omega = \pm 2t/\tau$ shows very similar behavior, as compared to the previous case of nontrivial fusion.

APPENDIX B: ANALYTIC CALCULATION OF LOCAL DENSITY OF STATES FOR A FOUR-SITE KITAEV HAMILTONIAN

In this Appendix, we calculate analytically the results for the four-site quantum dots at the sweet spot ($t_h = \Delta = 1$) to find the exact peak positions during the fusion process. The four-site Kitaev model without any coupling between the left and right quantum-dot arrays can be written as

$$H^L = -t_h c_1^\dagger c_2 + \Delta c_1 c_2 + \text{H.c.}, \tag{B1}$$

$$H^R = -t_h c_3^\dagger c_4 + \Delta c_3 c_4 + \text{H.c.} \tag{B2}$$

In the many-body basis ($2^4 = 16$ states), this four-site Hamiltonian is fourfold-degenerate with two states having total even parity, and the other two having odd parity. The fourfold-degenerate eigenvalues at $t_h = \Delta$ take the form $E_n = -2\Delta$. We have a total of four Majorana zero modes localized at each site, as shown in Fig. 7. The ground-state wave function in the presence of a very small interaction $V = 0.001$ (such that we have well-defined total parity) is

$$|\Psi_0\rangle = 0.5|0101\rangle + 0.5|0110\rangle + 0.5|1001\rangle + 0.5|1010\rangle. \tag{B3}$$

Note that the total fermion number parity of the system $P = \exp(i\pi \sum_j n_j) = +1$ (even), but the individual parity of the left and right quantum-dot segment is odd (as state kets take the form $|01\rangle \otimes |10\rangle$).

Next, we introduce the hopping and pairing coupling between the left and right quantum dots as a parameter:

$$H^C = -t_{23}^h c_2^\dagger c_3 + \Delta_{23} c_2 c_3 + \text{H.c.} \tag{B4}$$

FIG. 6. (a) Schematic representation of a 12-site quantum-dot array with different left and right superconducting pairing strength $\Delta_1 = 0.7$ and $\Delta_2 = 1.0$. The left part has overlapping quasi-MZMs (γ_1', γ_2') as the system is away from the sweet spot. The right part has nonoverlapping MZMs (γ_3, γ_4) and has $t_h = \Delta_2 = 1$. At time $t = 0$, there is no hopping and no pairing coupling between the Majoranas γ_2' and γ_3. (b) The electron component $LD_j^e(\omega, t)$ and (c) the hole component $LD_j^h(\omega, t)$, at site $j = 6$ and for different times t, all at $V = 0.05$. (d) The electron component $LD_j^e(\omega, t, j)$ and (e) the hole component $LD_j^h(\omega, t)$, at site $j = 7$ and for different times t, all at $V = 0.05$.

APPENDIX A: NONTRIVIAL FUSION BETWEEN A PAIR OF QUASI-MZMs AND A PAIR OF MZMs

In Fig. 6, we present the nontrivial fusion for 1D quantum dots with different pairing strengths $\Delta_1 = 0.7$ and $\Delta_2 = 1.0$. As the left part is away from the sweet spot, the MZMs (γ_1' and γ_2') spatially overlap with each other and move slightly away from zero energy [see Figs. 6(b) and 6(c)]. On the other hand, the right MZM pair (γ_3 and γ_4) are at sweet spot $\Delta_2 = t_h = 1$ and they do not overlap with each other. For the pairs on the right, we find equal-height peaks at $\omega = 0$ in the electron and hole parts of the local density of states at $t = 0$ [Figs. 6(d) and 6(e)]. This is expected for the MZMs as they are their own antiparticles, with an equal contribution of electron and hole components [32]. For $t > 0$, we vary the time-dependent

For finite values of $t_{23}^h = \Delta_{23}$ the fourfold degeneracy of the system splits into two pairs $[(E_1, E_2)$ and $(E_3, E_4)]$ of twofold-degenerate states with a combination of even and odd fermion parity. The four lowest eigenvalues are

$$E_1 = -2\Delta - \Delta_{23}, \quad \text{(B5)}$$

$$E_2 = -2\Delta - \Delta_{23}, \quad \text{(B6)}$$

$$E_3 = -2\Delta + \Delta_{23}, \quad \text{(B7)}$$

$$E_4 = -2\Delta + \Delta_{23}. \quad \text{(B8)}$$

We found that the ground-state wave function for finite values of $\Delta_{23} = 0.2$ (in units of t_h unless otherwise stated) (and very small values of $V = 0.001$) can be written as

$$|\Psi_0\rangle = 0.353|0000\rangle + 0.353|0011\rangle + 0.353|0101\rangle$$
$$+ 0.353|0110\rangle + 0.353|1001\rangle + 0.353|1010\rangle$$
$$+ 0.353|1100\rangle + 0.353|1111\rangle. \quad \text{(B9)}$$

Interestingly, now for the ground state $|\Psi_0\rangle$, the left and right parts of the quantum-dot segments have both even- and odd-parity kets, which allow for the formation of both electron and hole components in equal magnitude. The electron part of the local density of states at site j can be calculated as

$$LD_j^e(\omega, j) = -\frac{1}{\pi}\text{Im}\left(\sum_m \frac{\langle\Psi_1|c_j^\dagger|\Psi_m\rangle\langle\Psi_m|c_j|\Psi_1\rangle}{\omega + E_m - E_1 + i\eta}\right). \quad \text{(B10)}$$

We find that the peaks in the electron or hole portions of the local density of states arise from the transition between the states ($m = 3$ and 1) with opposite fermion parity. The peak position for $\Delta_{23} = 0.2$ in the electron part of the local density of states appears at $\omega = E_1 - E_3 = -2\Delta_{23} = -0.4$. Similarly for the hole part of the local density of states, the peak appears at $\omega = E_3 - E_1 = 2\Delta_{23} = +0.4$. For the static case in the nontrivial fusion process, these results show that we have the formation of an electron at $\omega = -2\Delta_{23}$ and a hole at $\omega = +2\Delta_{23}$. The peak heights in the electron and hole parts of the local density of states are almost the same, indicating the formation of an equal magnitude of electron and hole in the nontrivial fusion process [44].

APPENDIX C: THE OVERLAP OF TIME-EVOLVING WAVE FUNCTIONS WITH OTHER LOW-ENERGY STATES

1. $\phi_1 = \phi_2 = 0$

In Fig. 8, we calculate the overlap of the time-evolving states $|\Psi(t)\rangle$ with the four lower states of the instantaneous Hamiltonian $H(t)$ in the processes of nontrivial fusion of MZMs. We start the time evolution using the ground state $|\Psi(0)\rangle$ with total parity $P = +1$ of the system shown in Fig. 8(a), where both the left and right parts of the quantum-dot arrays have the same superconducting phases $\phi_1 = \phi_2 = 0$ and $t_h = |\Delta| = 1$. At time $t = 0$, there is no hopping and no pairing coupling between the left and right quantum-dot
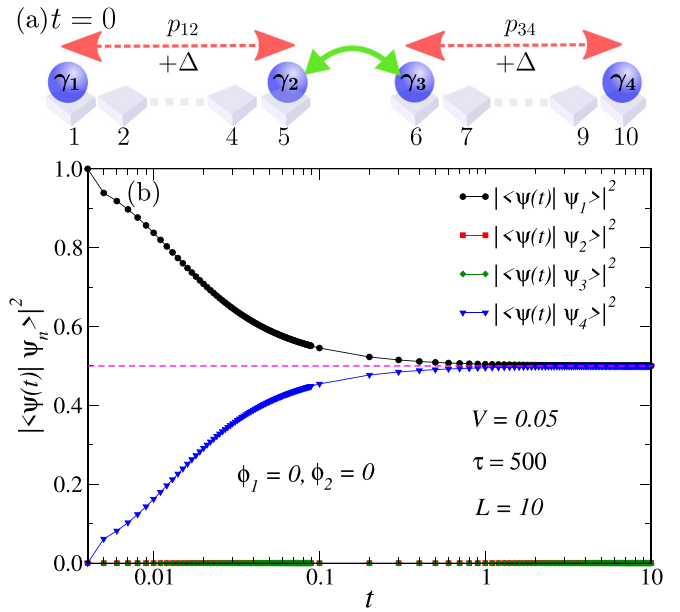

FIG. 8. (a) Schematic representation of two pairs of MZMs using a 10-site quantum-dot array with the same left and right superconducting phases $\phi_1 = \phi_2 = 0$. At time $t = 0$, there is no hopping and no pairing coupling between the Majoranas γ_2 and γ_3. (b) The overlap of time-evolving wave function $|\Psi(t)\rangle$ with the four lowest states of the instantaneous Hamiltonian at time t (in log scale). The numerical calculations were performed using the full diagonalization of an $L = 10$-site cluster and $V = 0.05$, $\tau = 500$.

segments [Fig. 8(a)]. As described in the main text, we perform the time evolution by changing the hopping according to the formula $t_h(t) = t_h(T)\frac{n\delta t}{\tau}$ using a system size $L = 10$ sites and $\tau = 500$. As shown in Fig. 8(b), the time-evolving states $|\Psi(t)\rangle$ becomes an equal superposition of two states $|\Psi_1\rangle$ and $|\Psi_4\rangle$ very shortly with an increase in time. Note that the individual total parity of the $|\Psi_1\rangle$ and $|\Psi_4\rangle$ states is the same as in the case of the time-evolving states $|\Psi(t)\rangle$. The equal superposition of these two states $|\Psi_1\rangle$ and $|\Psi_4\rangle$ results in an equal amount of spectral weight at $\omega = \pm 2t/\tau$ in both electron and hole parts of the local density of states.

2. $\phi_1 = \pi$ and $\phi_2 = 0$

In Fig. 9, we consider a π-junction quantum-dot array, where both the left and right parts of the system have different superconducting phases $\phi_1 = \pi$ and $\phi_2 = 0$. The parameters are $t_h = |\Delta| = 1$. We start the time evolution using the ground state $|\Psi(0)\rangle$ with total parity $P = +1$ of the system shown in Fig. 9(a). At time $t = 0$, there is no hopping and no pairing coupling between the left and right quantum-dot segments [Fig. 9(a)]. Next, we calculate the overlap of the time-evolving sites, using $\tau = 100$. As shown in Fig. 9(b), the time-evolving states $|\Psi(t)\rangle = u|\Psi_1\rangle + v|\Psi_4\rangle$ become a superposition of two low-energy degenerate ground states (with the same total parity). The amplitudes u and v depend on the tunneling of the MZM γ_3 from site $j = 6$ to site $j = 4$ and change far more slowly as compared to the case when $\phi_1 = \phi_2 = 0$. Interestingly, the system remains fourfold-degenerate even with the change with time in $t_h(t) = \Delta(t)$ at the bond between site
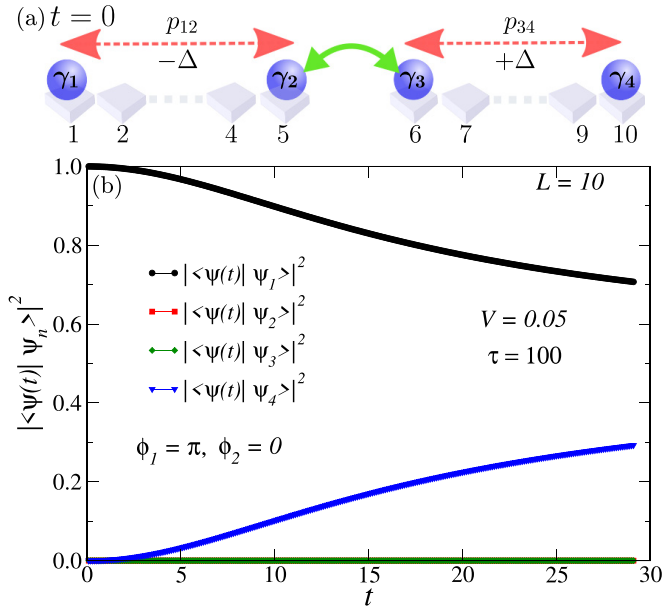
FIG. 9. (a) Schematic representation of two pairs of MZMs using a 10-site quantum-dot array with different left and right superconducting phases $\phi_1 = \pi$ and $\phi_2 = 0$. At time $t = 0$, there is no hopping and no pairing coupling between the Majoranas γ_2 and γ_3. (b) The overlap of the time-evolving wave function $\Psi(t)$ with the four lowest states of the instantaneous Hamiltonian at time t. The numerical calculations were performed using full diagonalization of $L = 10$ sites and $V = 0.05$, $\tau = 100$.

$j = 5$ and 6. This result shows that in the case of the tunneling of MZM through a localized Majorana at site $j = 5$, it still leads to a superposition of two low-energy states. Note that the amplitudes u and v remain the same for different values of large τ.
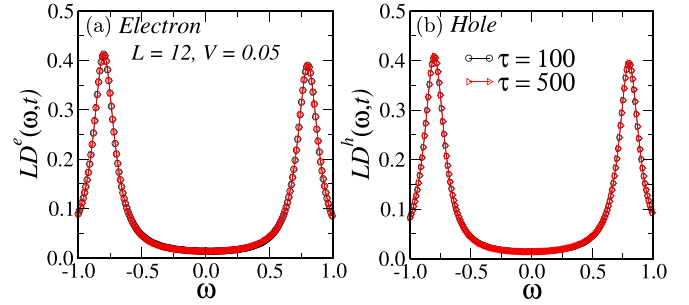

FIG. 10. Comparison of the local density of states at $t/\tau = 0.4$ and site $j = 6$, and for different values of $\tau = 100$ and 500: (a) electron part of the local density of states $LD_j^e(\omega, t)$, and (b) hole part of the local density of states $LD_j^h(\omega, t)$. These numerical calculations were performed using $L = 12$ sites and $V = 0.05$.

APPENDIX D: LOCAL DENSITY OF STATES FOR DIFFERENT VALUES OF THE QUENCH RATE $1/\tau$

In the main text of the paper, for the time evolution of the one-dimensional quantum-dot arrays, we used $\tau = 100$, which is already a quite small quench rate $1/\tau$. To confirm that this value characterizes an adiabatic process, in Fig. 10 we have compared the electron and hole parts of the local density of states at $t/\tau = 0.4$ for two different values of τ, i.e., $\tau = 100$ and 500. As shown in Fig. 10(a), the electron part of the local density of states at $\omega = \pm 2t/\tau = \pm 0.8$ remains the same for two different values of $\tau = 100$ and 500. Similarly, we also find that the hole part of the local density of states also takes the same values for two different values of $\tau = 100$ and 500. These results show that the quench rate $1/\tau$ considered in the main text ($\tau = 100$) is already a quite small number, representative of adiabatic movement, and the dynamical results are unchanged even for larger values of τ.

[1] A. Y. Kitaev, Fault-tolerant quantum computation by anyons, Ann. Phys. **303**, 2 (2003).

[2] S. Sarma, M. Freedman, and C. Nayak, Majorana zero modes and topological quantum computation, npj Quantum Inf. **1**, 15001 (2015).

[3] C. Nayak, S. H. Simon, A. Stern, M. Freedman, and S. D. Sarma, Non-Abelian anyons and topological quantum computation, Rev. Mod. Phys. **80**, 1083 (2008).

[4] A. Y. Kitaev, Unpaired Majorana fermions in quantum wires, Phys. Usp. **44**, 131 (2001).

[5] M. S. Scheurer and A. Shnirman, Nonadiabatic processes in Majorana qubit systems, Phys. Rev. B **88**, 064515 (2013).

[6] T. Dvir, G. Wang, N. van Loo *et al.*, Realization of a minimal Kitaev chain in coupled quantum dots, Nature (London) **614**, 445 (2023).

[7] J. Sau and S. D. Sarma, Realizing a robust practical Majorana chain in a quantum-dot-superconductor linear array, Nat. Commun. **3**, 964 (2012).

[8] A. Tsintzis, R. S. Souto, and M. Leijnse, Creating and detecting poor man's Majorana bound states in interacting quantum dots, Phys. Rev. B **106**, L201404 (2022).

[9] A. R. Mills, D. M. Zajac, M. J. Gullans *et al.*, Shuttling a single charge across a one-dimensional array of silicon quantum dots, Nat. Commun. **10**, 1063 (2019).

[10] M. T. Deng, E. Vaitiekėnas, E. B. Hansen, J. Danon *et al.*, Majorana bound state in a coupled quantum-dot hybrid-nanowire system, Science **354**, 1557 (2016).

[11] M. J. Rančić, S. Hoffman, C. Schrade, J. Klinovaja, and D. Loss, Entangling spins in double quantum dots and Majorana bound states, Phys. Rev. B **99**, 165306 (2019).

[12] G. Wang, T. Dvir, G. P. Mazur, C.-X. Liu, N. van Loo *et al.*, Singlet and triplet Cooper pair splitting in superconducting-semiconducting hybrid nanowires, Nature (London) **612**, 448 (2022).

[13] Q. Wang, S. L. D. ten Haaf, I. Kulesh *et al.*, Triplet correlations in Cooper pair splitters realized in a two-dimensional electron gas, Nat. Commun. **14**, 4876 (2023).

[14] C.-X. Liu, G. Wang, T. Dvir, and M. Wimmer, Tunable superconducting coupling of quantum dots via Andreev bound states in semiconductor-superconductor nanowires, Phys. Rev. Lett. **129**, 267701 (2022).

[15] H. Pan and S. Das Sarma, Disorder effects on Majorana zero modes: Kitaev chain versus semiconductor nanowire, Phys. Rev. B **103**, 224505 (2021).

[16] A. Bordin, C.-X. Liu, T. Dvir, F. Zatelli, S. L. D. ten Haaf, D. van Driel, G. Wang, N. van Loo, T. van Caekenberghe, J. C. Wolff, Y. Zhang, G. Badawy, S. Gazibegovic, E. P. A. M. Bakkers, M. Wimmer, L. P. Kouwenhoven, and G. P. Mazur, Signatures of Majorana protection in a three-site Kitaev chain, arXiv:2402.19382.

[17] D. Aasen, M. Hell, R. V. Mishmash, A. Higginbotham *et al.*, Milestones toward Majorana-based quantum computing, Phys. Rev. X **6**, 031016 (2016).

[18] J. Alicea, Y. Oreg, G. Refael, F. van Oppen, and M. P. A. Fisher, Non-Abelian statistics and topological quantum information processing in 1D wire networks, Nat. Phys. **7**, 412 (2011).

[19] M. Leijnse and K. Flensberg, Parity qubits and poor man's Majorana bound states in double quantum dots, Phys. Rev. B **86**, 134528 (2012).

[20] B. Pandey, N. Kaushal, G. Alvarez, and E. Dagotto, Majorana zero modes in Y-shape interacting Kitaev wires, npj Quantum Mater. **8**, 51 (2023).

[21] B. Pandey, N. Mohanta, and E. Dagotto, Out-of-equilibrium Majorana zero modes in interacting Kitaev chains, Phys. Rev. B **107**, L060304 (2023).

[22] T. Zhou, M. C. Dartiailh, K. Sardashti, J. E. Han, A. Matos-Abiague, J. Shabani and I. Žutić, Fusion of Majorana bound states with mini-gate control in two-dimensional systems, Nat. Commun. **13**, 1738 (2022).

[23] J. Bai, Q. Wang, L. Xu, W. Feng, and X.-Q. Li, Probing the non-Abelian fusion of a pair of Majorana zero modes, Phys. Rev. B **109**, 085403 (2024).

[24] C.-X. Liu, H. Pan, F. Setiawan, M. Wimmer, and J. D. Sau, Fusion protocol for Majorana modes in coupled quantum dots, Phys. Rev. B **108**, 085437 (2023).

[25] D. J. Clarke, J. D. Sau, and S. Das Sarma, Probability and braiding statistics in Majorana nanowires, Phys. Rev. B **95**, 155451 (2017).

[26] A. Tsintzis, R. S. Souto, K. Flensberg, J. Danon, and M. Leijnse, Majorana qubits and non-abelian physics in quantum dot–based minimal kitaev chains, PRX Quantum **5**, 010323 (2024).

[27] H. Zhang, D. E. Liu, M. Wimmer, and L. P. Kouwenhoven, Next steps of quantum transport in Majorana nanowire devices, Nat. Commun. **10**, 5128 (2019).

[28] A. Bordin, X. Li, D. V. Driel, J. C. Wolff, Q. Wang *et al.*, Crossed Andreev reflection and elastic co-tunneling in a three-site Kitaev chain nanowire device, arXiv:2306.07696.

[29] M. W. A. de Moor, J. D. S. Bommer, Di Xu, G. W. Winkler *et al.*, Electric field tunable superconductor-semiconductor coupling in Majorana nanowires, New J. Phys. **20**, 103049 (2018).

[30] C.-X. Liu, S. Miles, A. Bordin, S. L. D. ten Haaf, A. Mert Bozkurt, and M. Wimmer, Protocol for scaling up a sign-ordered Kitaev chain without magnetic flux control, arXiv:2407.04630.

[31] C. Chiu, M. M. Vazifeh, and M. Franz, Majorana fermion exchange in strictly one-dimensional structures, Europhys. Lett. **110**, 10001 (2015).

[32] J. Herbrych, M. Sroda, G. Alvarez, and E. Dagotto, Interaction-induced topological phase transition and Majorana edge states in low-dimensional orbital-selective Mott insulators, Nat. Commun. **12**, 2955 (2021).

[33] R. Thomale, S. Rachel, and P. Schmitteckert, Tunneling spectra simulation of interacting Majorana wires, Phys. Rev. B **88**, 161103(R) (2013).

[34] V. Svensson and M. Leijnse, Quantum-dot-based Kitaev chains: Majorana quality measures and scaling with increasing chain length, arXiv:2407.09211 v1.

[35] A. M. Turner, F. Pollmann, and E. Berg, Topological phases of one-dimensional fermions: An entanglement point of view, Phys. Rev. B **83**, 075102 (2011).

[36] G. Kells, D. Sen, J. K. Slingerland, and S. Vishveshwara, Topological blocking in quantum quench dynamics, Phys. Rev. B **89**, 235130 (2014).

[37] D. M. Kennes, C. Klöckner, and V. Meden, Spectral properties of one-dimensional fermi systems after an interaction quench, Phys. Rev. Lett. **113**, 116401 (2014).

[38] D. B. Karki, K. A. Matveev, and I. Martin, Physics of the Majorana-superconducting qubit hybrids, Phys. Rev. B **109**, 085410 (2024).

[39] B. Pandey, G. Alvarez, E. Dagotto, and R.-X. Zhang, Crystalline-symmetry-protected Majorana modes in coupled quantum dots, arXiv:2407.00158.

[40] K. Flensberg, Tunneling characteristics of a chain of Majorana bound states, Phys. Rev. B **82**, 180516(R) (2010).

[41] V. T. Lahtinen and J. K. Pachos, A short introduction to topological quantum computation, SciPost Phys. **3**, 021 (2017).

[42] J. D. T. Luna, A. m. Bozkurt, M. Wimmer, and C.-X. Liu, Flux-tunable Kitaev chain in a quantum dot array, arXiv:2402.07575.

[43] B. Jäck, Y. Xie, and A. Yazdani, Detecting and distinguishing Majorana zero modes with the scanning tunnelling microscope, Nat. Rev. Phys. **3**, 541 (2021).

[44] R. S. Souto and R. Aguado, Subgap states in semiconductor-superconductor devices for quantum technologies: Andreev qubits and minimal Majorana chains, arXiv:2404.06592.